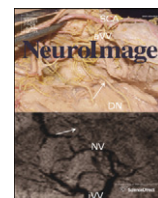


Contents lists available at [ScienceDirect](http://ScienceDirect.com)

NeuroImage

journal homepage: www.elsevier.com/locate/ynimg

Test–retest reproducibility of cannabinoid-receptor type 1 availability quantified with the PET ligand [¹¹C]MePPEP



Daniela A. Riaño Barros ^{a,b}, Colm J. McGinnity ^{a,b}, Lula Rosso ^a, Rolf A. Heckemann ^{a,e}, Oliver D. Howes ^{a,b}, David J. Brooks ^{a,f}, John S. Duncan ^{c,d}, Federico E. Turkheimer ^g, Matthias J. Koepp ^{c,d}, Alexander Hammers ^{a,b,c,d,e,*}

^a Centre for Neuroscience, Department of Medicine, Imperial College London, London, UK

^b MRC Clinical Sciences Centre Hammersmith Hospital, London, UK

^c Department of Clinical and Experimental Epilepsy, Institute of Neurology, University College London, UK

^d Epilepsy Society, Chalfont St Peter, UK

^e Neurodis Foundation, CERMEP, Imagerie du Vivant, Lyon, France

^f Institute of Clinical Medicine, Aarhus University, Denmark

^g Centre for Neuroimaging, Institute of Psychiatry, King's College London, London, UK

ARTICLE INFO

Article history:

Accepted 7 April 2014

Available online 13 April 2014

Keywords:

CB₁

Positron Emission Tomography

Reliability

Intra-class correlation coefficient

ABSTRACT

Background: Endocannabinoids are involved in normal cognition, and dysfunction in cannabinoid-receptor-mediated neurotransmission has been suggested in a variety of neurological and psychiatric pathologies. The type 1 cannabinoid receptor (CB₁) is widely expressed in the human central nervous system. The objective of this study was to quantify the test–retest reproducibility of measures of the PET ligand [¹¹C]MePPEP in order to assess the stability of CB₁-receptor quantification in humans in vivo.

Methods: Fifteen healthy subjects (eight females; median age 32 years, range 25 to 65 years) had a 90-minute PET scan on two occasions after injection of a median dose of [¹¹C]MePPEP of 364 MBq. Metabolite-corrected arterial plasma input functions were obtained for all scans. Eight ROIs, reflecting different levels of receptor densities/concentrations, were defined automatically: hippocampus, anterior cingulate gyrus, inferior frontal gyrus, caudate nucleus, globus pallidus, nucleus accumbens, thalamus, and pons. We used seven quantification methods: reversible compartmental models with one and two tissue classes, two and four rate constants, and a variable blood volume term (2kbv; 4kbv); model-free (spectral) analyses with and without regularisation, including one with voxel-wise quantification; the simplified reference tissue model (SRTM) with pons as a pseudo-reference region; and modified standard uptake values (mSUVs) calculated for the period of ~30–60 min after injection. Percentage test–retest change and between-subject variability were both assessed, and test–retest reliability was quantified by the intraclass correlation coefficient (ICC). The ratio of binding estimates pallidum:pons served as an indicator of a method's ability to reflect binding heterogeneity.

Results: Neither the SRTM nor the 4kbv model produced reliable measures, with ICCs around zero. Very good (>0.75) or excellent (>0.80) ICCs were obtained with the other methods. The most reliable were spectral analysis parametric maps (average across regions ± standard deviation 0.83 ± 0.03), rank shaping regularised spectral analysis (0.82 ± 0.05), and the 2kbv model (0.82 ± 0.09), but mSUVs were also reliable for most regions (0.79 ± 0.13). Mean test–retest changes among the five well-performing methods ranged from 12 ± 10% for mSUVs to 16% for 2kbv. Intersubject variability was high, with mean between-subject coefficients of variation ranging from 32 ± 13% for mSUVs to 45% for 2kbv. The highest pallidum:pons ratios of binding estimates were achieved by mSUV (4.2), spectral analysis-derived parametric maps (3.6), and 2kbv (3.6).

Conclusion: Quantification of CB₁ receptor availability using [¹¹C]MePPEP shows good to excellent reproducibility with several kinetic models and model-free analyses, whether applied on a region-of-interest or voxelwise basis. Simple mSUV measures were also reliable for most regions, but do not allow fully quantitative interpretation. [¹¹C]MePPEP PET is well placed as a tool to investigate CB₁-receptor mediated neurotransmission in health and disease.

Crown Copyright © 2014 Published by Elsevier Inc. This is an open access article under the CC BY license (<http://creativecommons.org/licenses/by/3.0/>).

* Corresponding author at: Neurodis Foundation, c/o CERMEP – Imagerie du vivant, 59 boulevard Pinel, 69677 Lyon/Bron, France. Fax: +33 4 72 68 86 10.

E-mail address: alexander.hammers@fondation-neurodis.org (A. Hammers).

Introduction

Endocannabinoids and their receptors are involved in a wide spectrum of conditions, e.g. addiction (Bossong et al., 2009) and epilepsy (Goffin et al., 2011), as well as in normal cognition (Hampson et al., 2011).

Two transmembrane G-protein coupled receptor types in the endocannabinoid system have been discovered. Type 1 (CB₁) is found in the central nervous system (CNS) and in neuronal and non-neuronal tissues outside the CNS (Matsuda et al., 1990). Abundantly expressed in presynaptic glutamatergic and GABAergic terminals (Katona and Freund, 2008), CB₁ receptors have a heterogeneous CNS distribution. High concentrations are found in the cerebral cortex, hippocampus, caudate nucleus and putamen, substantia nigra pars reticulata, globus pallidus, entopeduncular nucleus, the molecular layer of the cerebellum and in pain pathways of brain and spinal cord (Herkenham et al., 1990; Irving et al., 2002). However, the thalamus and most of the brainstem show low concentrations (Herkenham et al., 1990).

In the preclinical setting, a wide range of CB₁-selective radioligands have been used successfully in vitro, such as [³H]CP-55,940 (Devane et al., 1988, 1992), [³H]SR141716A (Petitet et al., 1996), and [³⁵S]GTPγS (Griffin et al., 1998); and also in vivo, such as (–)-5′-[¹⁸F]-Δ⁸-THC (Charalambous et al., 1991), [¹²³I]AM251 (Gatley et al., 1996), [¹²³I]AM281 (Gatley et al., 1998), [¹¹C]OMAR ([¹¹C]JHU75528) (Horti et al., 2006), [¹¹C]MePPEP (Yasuno et al., 2008), [¹¹C]/[¹⁸F]-PipISB (Finnema et al., 2009) and [¹¹C]CB-119 (Hamill et al., 2009). In vivo human brain CB₁ availability has recently become quantifiable with PET and the use of tracers such as [¹⁸F]MK-9470 (Burns et al., 2007), [¹¹C]OMAR (Wong et al., 2010), [¹¹C]MePPEP (Terry et al., 2009), and [¹⁸F]FMPEP-d₂ (G.E. Terry et al., 2010b).

MePPEP ((3R,5R)-5-(3-methoxy-phenyl)-3-((R)-1-phenylethylamino)-1-(4-trifluoro-methyl-phenyl)-pyrrolidin-2-one) is a CB₁-selective inverse agonist. [¹¹C]MePPEP has high and stable brain uptake in vivo. Despite its moderately high lipophilicity (measured LogD_{7.4} = 4.8) (Yasuno et al., 2008), its specific binding is relatively high with >85% in monkey brain and 65% determined using CB₁ knockout mouse brain (Terry et al., 2008, 2010b; Yasuno et al., 2008).

One reproducibility study with [¹¹C]MePPEP has been performed in humans so far, involving eight test–retest scans (Terry et al., 2009) after injection of high doses of [¹¹C]MePPEP (~650 MBq). Only standard uptake values and distribution volumes derived from compartmental modelling were examined.

In the present study we calculated the reproducibility of various parameters to describe CB₁ receptor availability with [¹¹C]MePPEP, including compartmental modelling techniques, spectral analysis variants, a simplified reference tissue model, and simple mSUVs, in regions representative of various CB₁ receptor concentrations in 15 healthy volunteers.

Materials and methods

Subjects

Ethical approval was obtained from the London – Surrey Borders Research Ethics Committee, and permission to undertake the study from the UK's radiation protection agency (ARSAC). Seventeen healthy subjects were recruited and gave written informed consent. Exclusion criteria were: history or presence of psychiatric or systemic medical condition, inability to provide informed consent, claustrophobia, any contraindication for undergoing MR, positive urine drug test, positive urine pregnancy test, general practitioner's (family doctor's) advice against participation, regular medication, use of cannabis within the previous three months or on more than five occasions over the subject's lifetime, and pathological modified Allen's test for patency of the ulnar artery (Allen, 1929; Cable et al., 1999; Slogoff et al., 1983). From this

sample two were excluded: one subject with pathological modified Allen's test; another withdrew consent for the retest scan. Hence, a total of fifteen healthy subjects (8 females; median age 32 years, range 25 to 65 years), without history of either systemic medical or psychiatric conditions or substance abuse were scanned twice. Demographic data are detailed in Table 1. All subjects underwent a urine drug screen cassette test for 11-nor-Δ⁹-THC, morphine, amphetamine, benzoylecgonine (the main metabolite of cocaine), methamphetamine and oxazepam (Monitect[®]; BMC, California, U.S.A.) prior to PET scanning. All female patients of childbearing age underwent a urine pregnancy test.

Radiochemistry

[¹¹C]MePPEP was synthesised on site by Hammersmith Imanet following a procedure described previously (Yasuno et al., 2008). Details of the injectate are listed in Table 1.

PET data acquisition

PET scans were acquired on a Siemens/CTI ECAT EXACT HR + 962 camera (Knoxville, TN, USA) in 3D mode. Ten-minute transmission scans for attenuation correction were obtained prior to dynamic emission scans using a rotating 137Cs point source. Each dynamic acquisition was 90 min long and consisted of 35 frames of increasing length (1 × 30", 6 × 10", 3 × 20", 3 × 30", 3 × 60", 6 × 120", 8 × 300" and 3 × 600"). 30 s after the scan start, [¹¹C]MePPEP was injected as an intravenous bolus injection of ~370 MBq (median 364 MBq, range 316–399 MBq; Table 1). Subjects were scanned on two separate days with a median interval of 24 days (range 1 to 309; Table 1).

The head position was maintained throughout and monitored with the camera's positioning laser. If movement was noticed, subjects were repositioned and underwent a second transmission scan at the end of the dynamic scan. To compensate for head movement during dynamic scans, we used a *post hoc* frame-by-frame realignment method, as described later (section "PET data quantification"). Data were reconstructed using FORE (Defrise et al., 1997) and 2D FBP (ramp filter, kernel 2.0 mm FWHM). Voxel sizes of reconstructed images were 2.092 × 2.092 × 2.42 mm.

Input function derivation

Continuous and intermittent blood samples were collected to allow the subsequent generation of metabolite-corrected arterial plasma time–activity curves (TACs) (Hammers et al., 2008). During the first 15 min blood was withdrawn continuously at a rate of 300 ml/h and radioactivity measured in a BGO detection system (Jones et al., 1994). To quantify plasma and whole blood radioactivity, as well as to allow quantification of the parent fraction of the radiotracer, intermittent discrete (10 ml) samples were taken with heparinised syringes before the scan (baseline) and at the following time points after scan start: 3, 5, 10, 15, 20, 30, and 50 min. At 75 min, a larger 17 ml sample was taken to allow quantification despite radioactivity decay. Parent fraction quantification was not possible at 90 min; hence at this time point only three millilitres was withdrawn for plasma and whole blood radioactivity measurement. Continuous plasma input functions (IF) were derived by cross-calibration and combination of the continuous and discrete data, multiplication with the fitted plasma-over-blood ratio, and correction for parent radiotracer fraction, as described in detail in previous studies (Hammers et al., 2007a; Jones et al., 1994).

MRI data acquisition, analysis and generation of ROIs

All subjects had 3D T1 weighted MRI scans with approximately millimetric voxel sizes on a Phillips Intera 3 Tesla (3 T) MRI scanner (Best, The Netherlands) at the Robert Steiner MRI Unit, Hammersmith

Table 1
Subjects' demographic and injectate details. BMI = Body Mass Index; Min = minimum; Max = maximum.

Subject no.	Age	Gender	BMI	Scan interval (days)	Dose (MBq)	Radiochemistry purity (%)	Co-injected mass (μ g)	Specific activity (MBq/nmol)
1	28	M	23	24	365	98	4.2	39
					364	98	6.2	27
2	44	M	28	23	375	96	3.0	56
					376	99	4.3	40
3	42	M	25	122	356	96	2.3	70
					373	100	2.3	72
4	26	M	24	1	361	98	3.4	48
					366	98	2.7	61
5	31	M	24	19	353	98	4.2	38
					355	99	2.7	60
6	27	F	21	309	367	99	4.6	37
					363	97	1.7	99
7	32	F	36	37	351	100	3.2	50
					316	100	8.3	17
8	65	F	22	23	355	97	2.3	69
					371	96	4.0	42
9	27	M	22	67	369	98	3.9	43
					366	98	3.1	54
10	29	F	23	4	360	97	9.7	17
					364	100	5.8	29
11	57	M	30	30	373	97	2.9	60
					399	96	5.0	37
12	61	F	36	93	361	96	1.8	92
					349	96	1.6	97
13	63	F	29	12	384	97	3.5	50
					380	98	3.3	52
14	25	F	31	156	364	97	2.4	69
					357	100	4.4	37
15	62	F	24	10	362	97	1.4	122
					366	97	3.3	51
Median	32		24	24	364	98	3.3	98
Interquartile range (25th–75th)	27–61		23–30	12–93	356–372	97–99	2.4–4.3	38–69
Min	25		21	1	316	96	1.4	17
Max	65		36	309	399	100	9.7	122

Hospital, for co-registration and ROI definition. There was no visible structural abnormality on any of the T1-weighted images.

T1-weighted images were segmented into tissue classes using the statistical parametrical mapping software SPM8 (Statistical Parametric Mapping, Wellcome Trust Centre for Neuroimaging, UCL, London, www.fil.ion.ucl.ac.uk/spm) under MATLAB© 7.4 (MathWorks).

The T1-weighted images were also anatomically segmented using MAPER (multi-atlas propagation with enhanced registration; Heckemann et al., 2010). Using high-dimensional image registration, 30 MRI data sets, each associated with manually determined labels of 83 regions (Gousias et al., 2008; Hammers et al., 2003), were propagated to the target brain. Label fusion was used to obtain 83 regions of interest (ROIs) in target space (Heckemann et al., 2006).

The T1-weighted images and corresponding MAPER-derived individual segmentations as well as individual grey matter (GM) probability images were co-registered with each subject's corresponding processed PET summation image for test and retest scans separately. For the cortical ROIs, the individual atlases in PET space were then multiplied with the grey matter probability maps thresholded at 0.5 using Analyze© 8.1 biomedical imaging software (Mayo Clinic 2002). These regions of interest were then used to sample the dynamic or parametric images.

Manual delineation of the pons

Because the pons is not included in the 83 regions obtained via MAPER, we delineated it manually using Analyze 8.1 (Fig. 1).

We evaluated the test–retest reliability of the quantification methods (see “PET data quantification” section) in a selection of eight bilateral ROIs in total. We chose representative regions with high CB₁ receptor concentrations; the grey matter masked cortical structures — hippocampus, anterior cingulate gyrus, and inferior frontal gyrus; and

the subcortical structures in their entirety, i.e. not grey matter masked (Heckemann et al., 2011) — caudate nucleus, globus pallidus, and nucleus accumbens. In addition, two regions with low concentration of CB₁ receptors were evaluated: the thalamus and the manually defined (entire) pons. The data from left and right homologues were averaged prior to quantification.

PET data quantification

All dynamic PET images were de-noised and corrected for movements frame-by-frame using wavelets in Piwave 8.0 (Studholme et al., 1996; Turkheimer et al., 1999). The frame starting at 4 min (frame 10) was used as reference due to its high signal-to-noise ratio and likelihood of subjects staying still during the first minutes of the scan. The first 93 s (frames 1 to 6) were not motion corrected due to their low signal-to-noise ratio. The remaining frames (7 to 35) were automatically re-sliced and re-concatenated into a new dynamic image (Hammers et al., 2007a).

A binary contiguous mask encompassing the entire brain and extending approximately 10 mm beyond the outer cortical boundary was created semi-automatically using Analyze 8.1 and applied to both dynamic and summed radioactivity-weighted images (ADD images) to reduce computation time.

Regional quantification of distribution/binding/uptake was then performed. In all following analyses, assessment was based on the same ROIs. Binding parameters were calculated directly for the ROI TAC data, except in the “classic” spectral analysis, where the additional aim was the assessment of the quality of parametric maps for use in voxel-by-voxel analyses, and the parametric map itself was sampled using the same ROIs:

1. Compartmental models, requiring arterial IFs (section “Compartmental models, requiring 1 arterial IFs”):

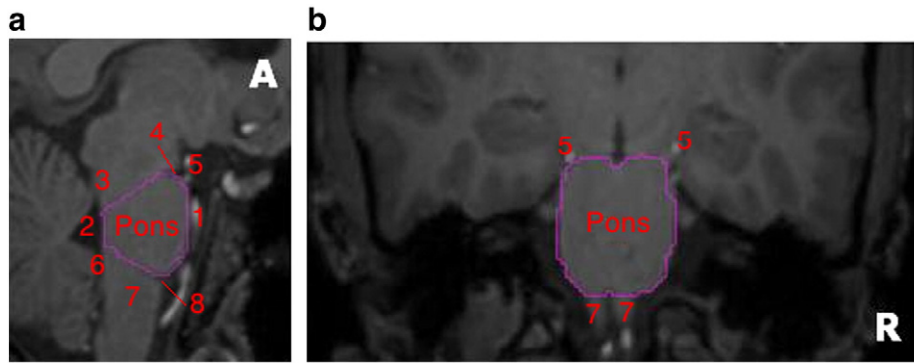


Fig. 1. Manual delineation of the pons on MRI. (a) Sagittal view, (b) coronal view, A – Anterior, R – right. The pons was first delineated on sagittal views, followed by coronal and axial views, with the following limits; anterior/ventral: cisterna interpeduncularis and basilar artery (1); posterior/dorsal: floor of the fourth ventricle (2); superior: a line was drawn from the floor of the fourth ventricle below the superior cerebellar peduncle (3) along the lower limit of the cerebral peduncle, to the indentation between the pons and the midbrain (4); inferior: a line was drawn from the floor of the fourth ventricle above the inferior peduncle (6) to the upper limits of the olive and pyramid of the medulla oblongata (7), i.e. to the indentation between the pons and medulla oblongata (8); on coronal view: following anatomical boundaries of pons, which are clearly visible; on axial view: following delineation in both sagittal and coronal views, the pons is now clearly delineated, and the axial view is used for verification. [5 – posterior cerebral artery].

- Reversible two-compartment (one tissue compartment) model with variable blood volume (2kbv) (section “Reversible two-compartment (one tissue compartment) model with two rate constants and a variable blood volume (2kbv)”)
 - Reversible three-compartment (two tissue compartment) model with variable blood volume (4kbv) (section “Reversible three-compartment (two tissue compartment) model with four rate constants and a variable blood volume (4kbv)”)
2. Model-free analyses, requiring arterial IFs (section “Model-free analyses, requiring arterial IFs”):
 - “Classic” (non-regularised) spectral analysis (SA), applied to ROI time-activity data (section “Classic” (non-regularised) SA’).
 - “Classic” SA, applied on a voxel-by-voxel basis to create parametric maps of V_T , which were then sampled in the same ROIs as for the other methods (section “Sampling parametric V_T images obtained voxel-by-voxel using spectral analysis (“Classic” SA)”).
 - Rank shaping regularisation of spectral analysis (SA; section “Directly obtaining V_T values from ROI data with SA and rank shaping regularisation”)
 3. Methods not requiring arterial IFs (section “Methods not requiring an arterial IF”):
 - Simplified reference tissue model (SRTM) using pons as a pseudo-reference tissue (section “Simplified reference tissue model using pons as a pseudo-reference tissue”)
 - (Regional) modified standard uptake values (mSUVs) (section “Modified standard uptake values (mSUVs)”)

Compartmental models, requiring arterial IFs

Reversible two-compartment (one tissue compartment) model with two rate constants and a variable blood volume (2kbv). In this model, three microparameters are derived: K_1 is the influx of the ligand from the plasma to the tissue compartment containing free, non-specifically bound, and specifically bound ligand, k_2 is the efflux constant from the ROI back to plasma (Cunningham et al., 1991; Huang et al., 1980), and bv is a variable blood volume term. V_T is then calculated according to the compartmental model equation (Watabe et al., 2006):

$$V_T = K_1/k_2. \quad (1)$$

Reversible three-compartment (two tissue compartment) model with four rate constants and a variable blood volume (4kbv). K_1 and k_2 were calculated as for the 2kbv compartmental model described above; in

addition, two additional rate constants were estimated to describe transfer relating to the third compartment: k_3 , which describes the transfer from the free and non-specifically bound compartment to the specifically bound (third) compartment; and k_4 , which describes the opposite transfer (Cunningham et al., 1991; Huang et al., 1980). Again, a variable blood volume term was also computed. According to compartmental model equations (Gunn et al., 2001; Watabe et al., 2006):

$$V_T = K_1/k_2(1 + k_3/k_4). \quad (2)$$

Model-free analyses, requiring arterial IFs

“Classic” (non-regularised) SA. Volumes of distribution (V_T s) (Innis et al., 2007) for each ROI were obtained from the dynamic images and the metabolite-corrected IFs using spectral analysis (SA) (Cunningham and Jones, 1993; Cunningham et al., 1993; Turkheimer et al., 1994). The fast frequency boundary was kept at the default value of 0.1 s^{-1} . The theoretical slow frequency boundary is given by the decay constant of ^{11}C ($t_{1/2} \approx 20 \text{ min}$, decay constant 0.0005663 s^{-1} ; $\log_{10} = -3.25$). Based on previous work with another tracer with relatively slow kinetics (Hammers et al., 2007a), we changed this to 0.00063 s^{-1} ($\log_{10} = -3.20$) in order to reduce noise.

Sampling parametric V_T images obtained voxel-by-voxel using spectral analysis (“Classic” SA). Parametric images of $[^{11}\text{C}]\text{MePPEP } V_T$ were obtained from the dynamic images and the metabolite-corrected IFs using spectral analysis (SA; Cunningham and Jones, 1993; Cunningham et al., 1993) and receptor parametric mapping software (RPM6; Aston et al., 2001; Gunn et al., 1997) with the same fast and slow frequency boundaries as above. The resulting parametric maps of V_T values were then sampled in the eight selected ROIs.

Directly obtaining V_T values from ROI data with SA and rank shaping regularisation. V_T values were generated directly from dynamic data sampled using ROIs with rank shaping (RS; orthogonalized-functional-base) regularisation of SA (Turkheimer et al., 2003) using in-house “Clickfit” software. As previously described by Turkheimer et al. (2003), we used the metabolite-corrected IF, a logarithmically spaced basis, an exponential range of bases extending to -3.2 , and the regional tissue TAC. TACs were weighted according to (Gunn et al., 1998):

$$W_i = L_i/T_i (\text{for frame } i = 1, 2, 3, \dots, 35) \quad (3)$$

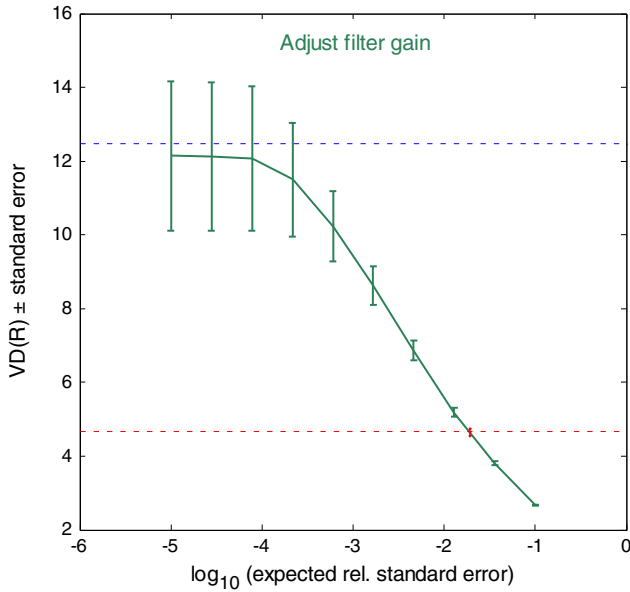


Fig. 2. Example plot showing a V_T of 12 obtained for the hippocampus from the $V_T(R)$ plateau (see section “Directly obtaining VT values from ROI data with SA and rank shaping regularisation”).

[w_i – weight for frame i ; L_i – length of frame i (seconds); and T_i – rate of true coincidences (per second)].

The V_T for each ROI was then obtained as the plateau of the $V_T(R)$, where R is the expected signal-to noise ratio that is used as the regularisation parameter (R) in rank-shaping (Fig. 2; (Turkheimer et al., 2003)).

Methods not requiring an arterial IF

Simplified reference tissue model using pons as a pseudo-reference tissue. CB_1 receptors are widespread in the brain, and a true reference region devoid of specific binding does not exist. A recent attempt to obviate the invasive procedure of arterial cannulation has been to use the ROI with the lowest receptor concentration as a pseudo-reference region

(Turkheimer et al., 2012). One of the structures with a low concentration of CB_1 receptors is the pons (Yasuno et al., 2008). We therefore used the pons as a pseudo-reference region in the simplified reference tissue model (SRTM).

Modified standard uptake values (mSUVs). Modified standard uptake values (mSUVs; Innis et al., 2007) for frames 25–31, i.e. from 29 min 50 s to 58 min 50 s after injection, were also derived for the ROIs according to (Goffin et al., 2011):

$$(\text{activity} \times [\text{weight}(\text{kg}) + 70 \text{ kg}]/2) / \text{injected dose.} \tag{4}$$

Global intensities (GI)

Global intensities (GI) were calculated with an in-house script derived from SPM (Hammers et al., 2007b), where the GI is defined as the mean voxel value within a mask defined as all voxels exceeding 1/8 of the mean value of all voxels in the image matrix.

Statistical analyses

For statistical testing we used SPSS© for Windows version 16 software (IBM 2008, New York, U.S.A.).

Injectate data were compared between test and retest sessions using the non-parametric Wilcoxon signed-rank test.

The percentage test–retest difference of parameters obtained with the various methods was calculated for all subjects in ROIs according to:

$$\frac{2 \cdot (\text{retest value} - \text{test value})}{\text{test value} + \text{retest value}} \cdot 100. \tag{5}$$

Reliability was calculated using intraclass correlation coefficients (Maclennan, 1993):

$$ICC = \frac{MSBS - MSWS}{MSBS + (dfWS \times MSWS)} \tag{6}$$

where MS = mean sum of squares, BS = between-subjects, WS = within-subjects, and df = degrees of freedom as computed in SPSS, using the “one-way random” model and reporting the “single

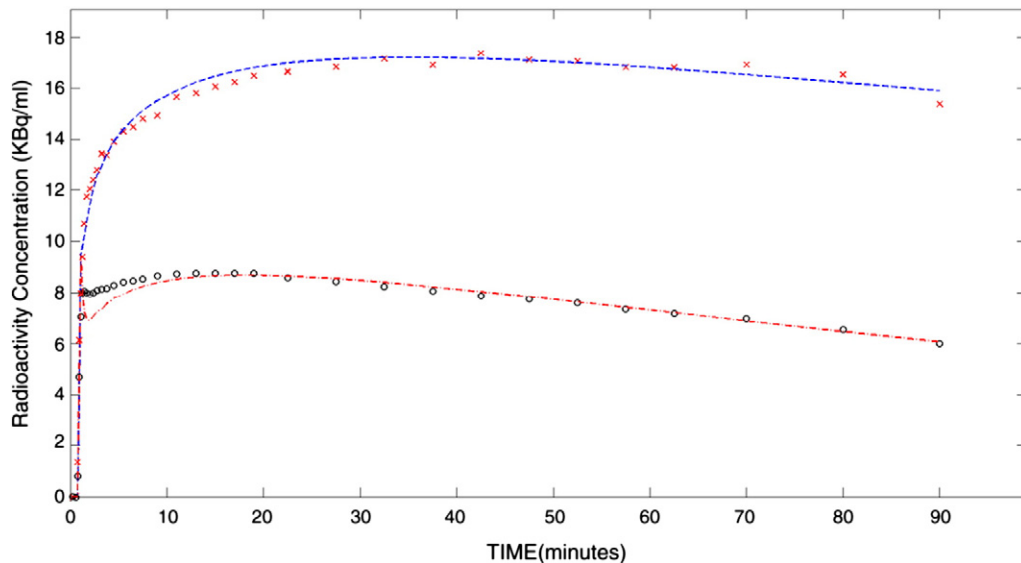


Fig. 3. Average time activity curves for the pallidum (top) and pons (bottom): the average uptake in each region as a function of time in minutes, subsequently fitted with a two-compartment (2kbv) model.

Table 2

Subjects' volume of distribution (V_T) obtained with two-compartment model (2kbv) method. ACG = anterior cingulate gyrus, IFG = inferior frontal gyrus, caudate = caudate nucleus, pallidum = globus pallidus, accumbens = nucleus accumbens. BS = between-subjects, CV = coefficient of variation, diff = difference, ICC = intraclass correlation coefficient, Min = minimum, Max = maximum, ROI = region-of-interest, SD = standard deviation.

ROI	Median	Interquartile range	Min	Max	Median % diff	Median % diff range	Mean BS % CV	ICC
Hippocampus	8.0	6.2–10.8	4.1	24.8	14.8	–54.8–54.2	50.4	0.88
ACG	10.3	7.5–14.0	1.0	26.4	27.8	–154.4–64.2	47.4	0.76
IFG	8.8	7.3–12.3	4.1	22.4	18.1	–48.3–31.9	42.1	0.83
Caudate	7.4	6.0–12.2	3.9	22.9	19.7	–60.9–33.5	48.0	0.85
Pallidum	10.8	8.5–14.2	1.1	32.6	20.6	–158.7–44.1	48.1	0.70
Accumbens	8.4	7.2–13.2	1.2	31.7	35.8	–150.5–51.5	53.7	0.69
Thalamus	5.1	4.4–7.3	2.9	10.9	12.6	–35.5–28.5	35.9	0.89
Pons	3.0	2.8–3.9	2.0	6.2	8.3	–10.7–20.2	30.2	0.95
				Mean	19.7		44.5	0.82
				(SD)	(8.7)		(7.9)	(0.09)

measures" ICC. ICC values ≥ 0.75 were considered indicators of good reliability (Portney and Watkins, 2009).

We used a Bland–Altman plot to compare methods and assess bias. In the Bland–Altman plot (also known as Tukey mean-difference plot), the average of two V_T measures for the same region is plotted on the x-axis, whereas the first V_T minus the second V_T is plotted on the y axis.

$$V_T(\mathbf{x}, \mathbf{y}) = \left(\frac{V_{T1} + V_{T2}}{2}, V_{T1} - V_{T2} \right)$$

Where quantification from two methods is in close agreement and without bias, the datapoints will be scattered close to $y = 0$, equally above and below the x axis. In this case, the 2kbv model was used as the reference, i.e. V_{T2} was always the average derived from 2kbv.

The association between percentage test–retest difference and interscan interval was quantified for the method yielding the highest ICCs using Spearman's rho correlation coefficient, with correction for multiple comparisons (8 regions) using the Bonferroni method. The volumes of distribution between genders were also compared using a repeated measures full-factorial general linear model, for the same method.

Results

Injectate

Details are given in Table 1. There were no significant differences between test and retest studies in terms of the amount of injected radioactivity (median (i.q.r)): test 362 (358–368) MBq; retest 366 (360–372) MBq; co-injected mass of stable ligand: test: 3.2 (2.4–4.1) μg , retest 3.3 (2.7–4.7) μg ; and specific activity at the time of injection: test 50 (49–61) MBq/ ηmol , retest: 51 (37–61) MBq/ ηmol .

Table 3

Subjects' V_T obtained with three-compartment model (4kbv). ACG = anterior cingulate gyrus, IFG = inferior frontal gyrus, caudate = caudate nucleus, pallidum = globus pallidus, accumbens = nucleus accumbens. BS = between-subjects, CV = coefficient of variation, diff = difference, ICC = intraclass correlation coefficient, Min = minimum, Max = maximum, ROI = region-of-interest, SD = standard deviation.

ROI	Median	Interquartile range	Min	Max	Median % diff	Median % diff range	Mean BS % CV	ICC
Hippocampus	13.4	7.5–19.6	–0.7	102.2	72.8	–219.9–175.6	81.1	–0.05
ACG	9.0	5.8–13.6	1.4	65.6	53.7	–136.2–126	81.4	0.23
IFG	8.9	4.7–11.2	0.8	18.6	61.1	–159–116.4	51.9	0.13
Caudate	6.2	4.2–8.5	0.0	31.5	68.5	–153.4–200.0	69.9	–0.13
Pallidum	10.6	6.7–18.3	3.4	79.8	69.7	–170.7–126.1	111.3	–0.03
Accumbens	13.6	8.7–39.5	0.0	163.5	122.1	–72.3–200.0	131.7	–0.06
Thalamus	6.1	4.5–8.4	1.2	30.5	32.7	–133.8–102.5	87.9	0.49
Pons	5.3	3.9–7.2	2.4	23.0	40.3	–23.4–146.5	79.0	0.50
				Mean	65.1		86.8	0.14
				(SD)	(27.1)		(24.6)	(0.25)

Image data

Global intensities of summed radioactivity images did not differ between test and retest studies (median, interquartile 25th–75th: test: 1.2, 1.0–1.6; retest: 1.3, 1.1–1.5; $p > 0.6$). Fig. 3 shows examples of time–activity curves.

Quantification results

The following sections describe the regional estimates for the parameters derived with the seven quantification methods. To assess test–retest variation, for each ROI the median percent difference between test and retest studies as well as their signed range is given in the tables. The coefficient of variation (standard deviation divided by the mean) quantifies the between-subject variability of the measure. The ICC assesses the reliability of the measure as a function of both within-subject variability and between-subject variability; the closer to the value of 1, the more reliable the method, i.e. the smaller the intra-subject variability of the measure compared with natural between-subject variability. Finally, the ratio of the generally highest binding region (pallidum) over the lowest binding region (pons) assesses a method's ability to reflect known binding heterogeneity.

A comparison of analysis methods and a synthetic overview of the various measures will be provided in the section "Comparison between analysis methods".

Compartmental models, requiring arterial IFs

Reversible two-compartment (one tissue compartment) model with variable blood volume (2kbv). The region with the highest V_T was globus pallidus (10.8; Table 2). Regional heterogeneity of V_T values was high, with a ratio of pallidum:pons of 3.6. ICCs ranged between 0.69 and 0.95, with a mean \pm SD of 0.82 ± 0.09 .

Table 4

Subjects' volume of distribution (V_T) obtained with Spectral Analysis (SA) based on ROI data. ACG = anterior cingulate gyrus, IFG = inferior frontal gyrus, caudate = caudate nucleus, pallidum = globus pallidus, accumbens = nucleus accumbens. BS = between-subjects, CV = coefficient of variation, diff = difference, ICC = intraclass correlation coefficient, Min = minimum, Max = maximum, ROI = region-of-interest, SD = standard deviation.

ROI	Median	Interquartile range	Min	Max	Median % diff	Median % diff range	Mean BS % CV	ICC
Hippocampus	12.4	9.4–17.2	6.6	23.4	10.9	–39.3–29.6	34.1	0.87
ACG	14.4	11.9–19.9	7.3	27.1	12.4	–64.3–39.3	35.0	0.74
IFG	13.9	10.1–19.3	5.4	26.3	13.3	–76.3–47.3	39.0	0.71
Caudate	13.0	9.3–19.4	5.9	28.1	13.6	–80.8–26.3	44.2	0.74
Pallidum	15.7	12–21.7	8.2	28.9	9.4	–53.8–33.5	35.5	0.85
Accumbens	13.9	11.3–18.9	6.9	26.7	15.1	–63.6–47.1	35.2	0.80
Thalamus	9.6	6.9–12.2	4.8	20.3	24.7	–60.7–49.2	39.4	0.70
Pons	6.0	4.6–7.1	2.9	11.8	24.8	–62.0–39.9	35.5	0.67
				Mean	15.5		37.2	0.76
				(SD)	(6.0)		(3.4)	(0.07)

Reversible three-compartment (two tissue compartment) model with variable blood volume (4kbv). The method yielded highly variable data. Unlike for the other methods, the regions with the highest V_T values were nucleus accumbens (13.6; Table 3) and hippocampus (13.4). The ratio of pallidum/pons was 2.0. ICCs ranged between –0.13 and 0.50, with a mean \pm SD of 0.14 ± 0.25 .

Model-free analyses, requiring arterial IFs

Directly obtaining V_T values from ROI data with “classic” spectral analysis (SA). The region with the highest V_T values was globus pallidus (15.7; Table 4). Regional heterogeneity of V_T values, estimated as the ratio of pallidum over pons, was 2.6. ICCs ranged between 0.67 and 0.87, with a mean \pm SD of 0.76 ± 0.07 .

Sampling parametric V_T images obtained with “classic” spectral analysis. The region with the highest V_T was the pallidum (15.8; Table 5). Regional heterogeneity of V_T values was moderate, with a ratio of pallidum over pons of 3.6. ICCs were fairly homogenous between regions and ranged between 0.76 and 0.87, with a mean \pm SD of 0.83 ± 0.03 . Fig. 4 shows an example of a parametric map.

Spectral analysis with rank shaping regularisation. The region with the highest V_T values was globus pallidus (10.3; Table 6). Regional heterogeneity of V_T values was lower than with the preceding methods, with a ratio of pallidum over pons of 2.4. ICCs ranged between 0.73 and 0.90, with a mean \pm SD of 0.82 ± 0.05 .

Methods not requiring an arterial IF

SRTM with pons as a pseudo-reference tissue. The method yielded inconsistent data. The regions with the highest values were the globus pallidus, the anterior cingulate gyri, and the nucleus accumbens ($BP_{ND} = 1.1$; Table 7). The ratio of pallidum over pons could not be

calculated, as the BP_{ND} of pons as the reference region is ~ 0 . ICCs ranged between –0.29 and 0.50, with a mean \pm SD of 0.07 ± 0.27 .

Modified standard uptake values (mSUVs). The region with the highest values was globus pallidus (3.6; Table 8). Regional heterogeneity of values was the highest of all methods tested with the ratio of pallidum over pons 4.2. ICCs ranged from 0.47 to 0.86, with a mean \pm SD of 0.79 ± 0.13 .

Comparison between analysis methods

Relative to the 2kbv model, a bias towards overestimation of medium high hippocampal V_T of [^{11}C]MePPEP was seen for both analyses using “classic” SA (Fig. 5). RS-SA did not show this bias but restricted the range of V_T estimates, with an underestimation of the highest V_T s. The 4kbv model was not assessed due to its lack of reliability.

Table 9 provides an overview of the median test–retest differences (%) for the different methods. 2kbv and the methods using SA had median differences between 13 and 20%, similar across regions as indicated by low spreads (SDs), whilst mSUVs varied even less on average, but with more between-region variation due to the pons showing high test–retest differences (37%). 4kbv and SRTM were very variable for most regions.

Mean between-subject coefficients of variation (BSCV; %) for the different methods are listed in Table 10. The between-subject variability based on mSUVs (i.e. tissue data only) was approximately 32%; however the BSCV for pons was 63%. The three methods based on SA had similar between-subject variation, around 36%, with similar variability for the various regions. Between-subject variability was higher for the 2kbv compartmental model, at 45%. SRTM and the 4kbv model yielded implausible values.

ICCs for all methods are listed in Table 11. As expected from the high test–retest variability (Table 9) and unrealistically high between-subject variability (Table 10), the 4kbv model and SRTM yielded non-

Table 5

Subjects' volume of distribution (V_T) obtained with “classic” spectral analysis (SA) on parametric maps. ACG = anterior cingulate gyrus, IFG = inferior frontal gyrus, caudate = caudate nucleus, pallidum = globus pallidus, accumbens = nucleus accumbens. BS = between-subjects, CV = coefficient of variation, diff = difference, ICC = intraclass correlation coefficient, Min = minimum, Max = maximum, ROI = region-of-interest, SD = standard deviation.

ROI	Median	Interquartile range	Min	Max	Median % diff	Median % diff range	Mean BS % CV	ICC
Hippocampus	11.5	9–16.2	7.0	22.6	9.6	–40.1–20.6	34.2	0.87
ACG	14.8	11.1–20.5	8.1	28.8	12.5	–44.0–30.1	34.7	0.85
IFG	14.8	10.4–20.3	7.6	27.6	12.0	–49.7–27.0	37.0	0.85
Caudate	12.9	10.2–19.3	6.5	26.9	12.3	–76.6–24.3	40.0	0.81
Pallidum	15.8	11.6–21.1	8.6	30.4	12.6	–53.0–23.5	35.4	0.83
Accumbens	9.5	7.8–13.9	5.3	18.7	12.3	–44.6–31.4	36.0	0.83
Thalamus	13.2	10.4–17.3	5.2	26.5	16.8	–78.9–50.8	37.1	0.76
Pons	4.4	3.5–5.3	1.7	9.6	20.2	–33.1–43.3	39.0	0.81
				Mean	13.5		36.7	0.83
				(SD)	(3.3)		(2.0)	(0.03)

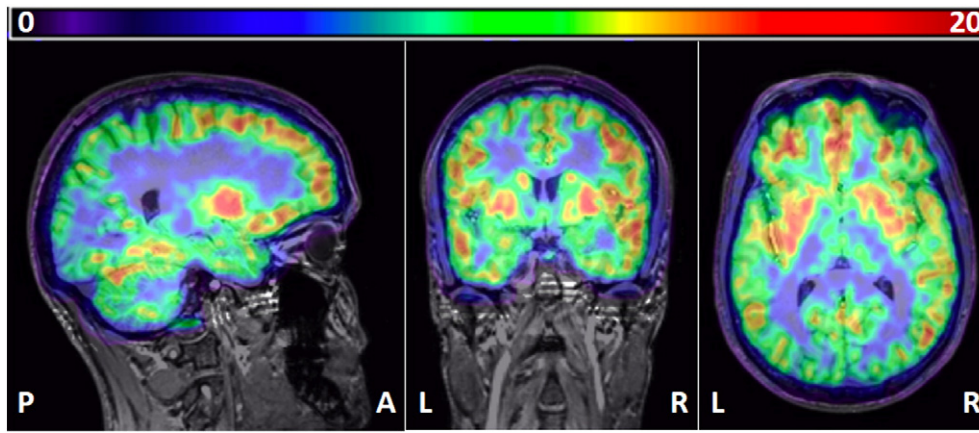


Fig. 4. Example of a parametric map, co-registered onto the subject's MRI scan. Left, sagittal; middle, coronal; right, transverse. Note high binding in the putamen and pallidum and intermediate binding in the hippocampus and thalamus. Colour bar: V_T values. P, posterior; A, anterior; R, right; L, left.

Table 6

Subjects' Volume of distribution (V_T) obtained with Rank Shaping (RS) regularisation of Spectral Analysis (SA) method. ACG = anterior cingulate gyrus, IFG = inferior frontal gyrus, caudate = caudate nucleus, pallidum = globus pallidus, accumbens = nucleus accumbens. BS = between-subjects, CV = coefficient of variation, diff = difference, ICC = intraclass correlation coefficient, Min = minimum, Max = maximum, ROI = region-of-interest, SD = standard deviation.

ROI	Median	Interquartile range	Min	Max	Median % diff	Median % diff range	Mean BS % CV	ICC
Hippocampus	8.2	5.8–10.4	4.2	15.2	14.4	–48.5–34.9	35.9	0.81
ACG	9.9	7.6–13.7	5.5	18.8	14.6	–29.7–32.4	34.0	0.86
IFG	9.9	7.2–13.8	5.3	18.2	15.6	–39.5–29.0	34.8	0.85
Caudate	8.1	6.1–12.6	4.4	18.1	11.6	–88.7–27.0	42.2	0.82
Pallidum	10.3	7.0–13.0	4.5	20.7	23.3	–64.1–42.3	39.7	0.77
Accumbens	8.6	6.1–10.5	3.2	15.9	18.5	–77.8–58.4	36.5	0.73
Thalamus	6.5	5.5–9.4	3.5	12.7	14.9	–43.9–31.0	34.7	0.85
Pons	4.3	3.3–5.3	2.5	8.0	7.4	–30.6–24.1	32.3	0.90
				Mean	15.0		36.3	0.82
				(SD)	(4.7)		(3.2)	(0.05)

reproducible results, as reflected by an ICC around zero. All the other methods had good to very good reproducibility, ranging from 0.76 ± 0.07 for classic SA calculated on ROI data to 0.83 ± 0.04 for classic SA applied to parametric maps. Note the low between-region spread of the ICC for the five methods with good or very good reproducibility, meaning that reproducibility was good throughout the brain regions sampled.

Table 11 also shows the ratio between a high-binding region (pallidum) and a low-binding region (pons), indicating a method's ability to reflect the known between-region heterogeneity. mSUVs had the highest differential, followed by 2kbv model and SA applied to parametric maps.

A positive correlation was observed for test–retest difference and interscan interval in the inferior frontal gyrus ($p = 0.039$, Spearman's $\rho = 0.538$) and the caudate ($p = 0.033$, Spearman's $\rho = 0.550$). These correlations were rendered insignificant by correction for

multiple comparisons. There was no significant influence of gender on the V_T s ($F = 27.349$, $p = 0.995$). There was no significant interaction between gender and test–retest condition ($p = 0.120$).

Discussion

We describe the test–retest reproducibility of quantification for CB_1 -receptor availability, as assessed by [^{11}C]MePPEP PET, in 15 healthy human subjects. Our major finding is that good-to-excellent reproducibility of estimates of availability is achievable using either the one tissue compartment, two rate-constant kinetic model with a variable blood volume term; model-free analyses using spectral analysis variants; or simple scaled measures of radioactivity (mSUV).

The performance of the various methods was consistent between measures – those having low percentage test–retest variability also

Table 7

Subjects' binding potential (BP_{ND}) obtained with the SRTM and pons as a pseudo-reference region. ACG = anterior cingulate gyrus, IFG = inferior frontal gyrus, caudate = caudate nucleus, pallidum = globus pallidus, accumbens = nucleus accumbens. BS = between-subjects, CV = coefficient of variation, diff = difference, ICC = intraclass correlation coefficient, Min = minimum, Max = maximum, ROI = region-of-interest, SD = standard deviation.

ROI	Median BP_{ND}	Interquartile range	Min	Max	Median % diff.	Median % diff range	Mean %BS-CV	ICC
Hippocampus	1.0	0.8–1.7	0.4	12.8	54.6	–155.5–176.6	125.2	–0.06
ACG	1.1	0.9–1.2	0.7	3.4	40.2	–142.9–71.7	–574.1	0.50
IFG	0.9	0.9–1.0	0.0	1.7	16.0	–66.6–207.6	29.4	–0.29
Caudate	0.9	0.6–1.0	0.2	2.7	30.5	–137.5–45.4	48.8	0.06
Pallidum	1.1	1.0–1.3	0.1	1.6	9.4	–37.9–158.4	25.1	0.27
Accumbens	1.1	0.7–1.6	–0.2	18.2	53.0	–213.9–180.6	157.4	–0.15
Thalamus	1.0	0.5–6.2	0.4	10.4	42.3	–169.8–181.2	108.2	0.19
				Mean	35.1			0.07
				(SD)	(17.4)			(0.27)

Table 8

Subjects' modified standard uptake values (mSUV). ACG = anterior cingulate gyrus, IFG = inferior frontal gyrus, caudate = caudate nucleus, pallidum = globus pallidus, accumbens = nucleus accumbens. BS = between-subjects, CV = coefficient of variation, diff = difference, ICC = intraclass correlation coefficient, Min = minimum, Max = maximum, ROI = region-of-interest, SD = standard deviation.

ROI	Median	Interquartile range	Min	Max	Median % diff.	Median % diff range	Mean %BS-CV	ICC
Hippocampus	2.7	2.1–3.2	1.8	4.2	8.3	–22.6–34.4	27.4	0.84
ACG	3.2	2.6–3.8	2.0	5.2	8.8	–24.1–32.7	27.2	0.86
IFG	3.2	2.6–3.7	2.1	5.3	8.9	–22.4–35.1	27.3	0.86
Caudate	2.9	2.5–3.9	1.9	5.1	7.6	–58.1–30.3	30.1	0.79
Pallidum	3.6	2.7–4.1	2.2	5.5	11.1	–28.6–30.9	27.1	0.84
Accumbens	3.0	2.4–3.6	1.5	4.7	6.7	–65.7–33.7	27.9	0.80
Thalamus	2.7	2.2–3.2	1.7	4.3	8.1	–16.7–38.1	25.8	0.83
Pons	0.9	0.6–1.3	0.3	3.4	36.7	7.3–108.2	62.6	0.47
				Mean	12.0		31.9	0.79
				(SD)	(10.1)		(12.5)	(0.13)

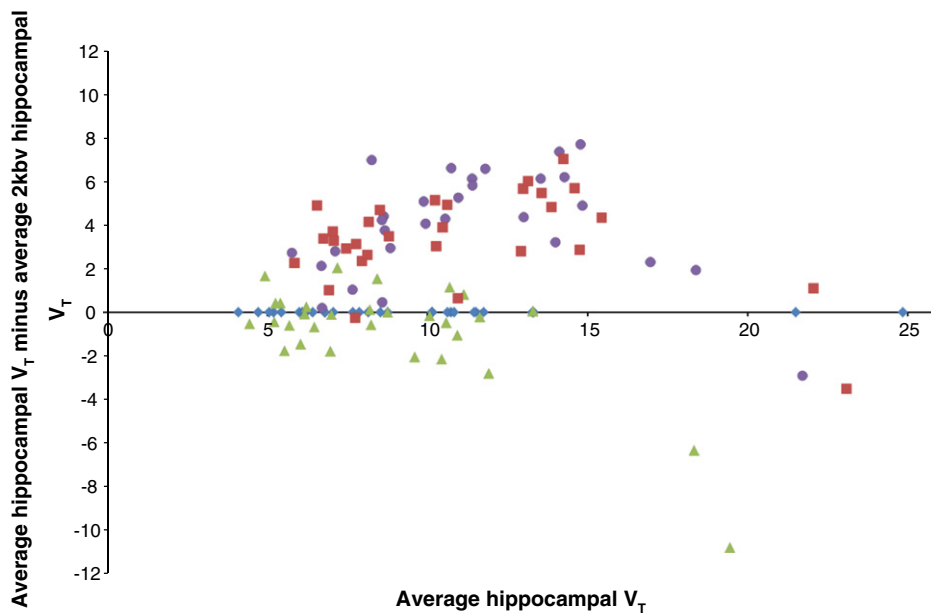


Fig. 5. Bland–Altman plot for the different methods to obtain V_T s. Data for the hippocampus is shown as an example, relative to the one compartment, two-rate constant model (blue diamonds, 2kbv); green triangles: rank-shaping regularisation of spectral analysis; red squares: “classic” voxel-wise SA; and purple circles: “classic” SA on ROI data.

had high ICCs, reflecting that among the well-performing methods, between-subject variability was comparable.

The 2kbv compartmental model was among the best performing methods for test–retest variability and reliability, and also had one of the highest ratios of pallidum over pons. This indicates low bias (i.e. a large range of concentrations between regions of known high and low

receptor availability). This ratio was lower for the spectral analysis variants applied to ROI data, reflecting their known bias towards lower V_T estimates in high binding regions (Hammers et al., 2007a). In contrast, voxel-wise SA had the same high pallidum/pons ratio as the 2kbv model. This may be due to SA’s ability to fit voxel-wise time courses – voxels with varying partial volume contributions of white matter or

Table 9

Median test–retest differences (%) for subjects' parameter estimates (V_T /BP_{ND}/mSUV) obtained with the different methods. ACG = anterior cingulate gyrus, IFG = inferior frontal gyrus, caudate = caudate nucleus, pallidum = globus pallidus, accumbens = nucleus accumbens. ROI = region-of-interest, SD = standard deviation.

Method	2kbv	4kbv	SA-ROIs	SA-maps	RS-SA	SRTM	mSUV
Parameter	V_T	V_T	V_T	V_T	V_T	BP _{ND}	kBq/ml
Sampling	ROI on dynamic images	ROI on dynamic images	ROI on dynamic images	ROI on parametric maps	ROI on dynamic images	ROI on dynamic images	ROI on summed images
Hippocampus	14.8	72.8	10.9	9.6	14.4	54.6	8.3
ACC	27.8	53.7	12.4	12.5	14.6	40.2	8.8
IFG	18.1	61.1	13.3	12.0	15.6	16.0	8.9
Caudate	19.7	68.5	13.6	12.3	11.6	30.5	7.6
Pallidum	20.6	69.7	9.4	12.6	23.3	9.4	11.1
Accumbens	35.8	122.1	15.1	12.3	18.5	53.0	6.7
Thalamus	12.6	32.7	24.7	16.8	14.9	42.3	8.1
Pons	8.3	40.3	24.8	20.2	7.4	NA	36.7
Mean ± SD	19.7 ± 8.7	65.1 ± 27.1	15.5 ± 5.9	13.5 ± 3.3	15.0 ± 4.6	35.1 ± 17.4	12.0 ± 10.1

Table 10

Mean between-subject coefficients of variation (BSCV; %) for subjects' V_T / BP_{ND} /mSUV parameters obtained with the different methods. ACG = anterior cingulate gyrus, IFG = inferior frontal gyrus, caudate = caudate nucleus, pallidum = globus pallidus, accumbens = nucleus accumbens. ROI = region-of-interest, SD = standard deviation, NA = not applicable.

Method	2kbv	4kbv	SA-ROIs	SA-maps	RS-SA	SRTM	mSUV
Parameter	V_T	V_T	V_T	V_T	V_T	BP_{ND}	kBq/ml
Sampling	ROI on dynamic images	ROI on dynamic images	ROI on dynamic images	ROI on parametric maps	ROI on dynamic images	ROI on dynamic images	ROI on summed images
Hippocampus	50.4	81.1	34.1	34.2	35.9	125.2	27.4
ACG	47.4	81.4	35.0	34.7	34.0	−574.1	27.2
IFG	42.1	51.9	39.0	37.0	34.8	29.4	27.3
Caudate	48.0	69.9	44.2	40.0	42.2	48.8	30.1
Globus Pallidum	48.1	111.3	35.5	35.4	39.7	25.1	27.1
Accumbens	53.7	131.7	35.2	36.0	36.5	157.4	27.9
Thalamus	35.9	87.9	39.4	37.1	34.7	108.2	25.8
Pons	30.2	79.0	35.5	39.0	32.3	NA	62.6
Mean ± SD	44.5 ± 7.9	86.8 ± 24.6	37.2 ± 3.4	36.7 ± 2.0	36.3 ± 3.2	−11.4 ± 253.2	31.9 ± 12.5

vasculature can be individually fitted, which is not the case for methods using the averaged ROI TAC.

Several, but not all (e.g. Ahmad et al., 2014; Goffin et al., 2011; Van Laere et al., 2010), earlier in vivo human studies with [^{18}F]MK-9470 (Burns et al., 2007), [^{11}C]MePPEP (Terry et al., 2009) and [^{18}F]FMPEP- d_2 (Terry et al., 2010b) involved 120 to 300 min scan times (Terry et al., 2009, 2010). This requirement limits the usefulness of these authors' approaches, as patients with debilitating conditions and even healthy volunteers are unlikely to tolerate PET scans of 2 h duration or more. Here we present data that indicates that with [^{11}C]MePPEP, reliable quantification of CB_1 receptor availability is achievable with just 90 min of data acquisition. In a previous study, it has been shown that 90 min of acquisition is sufficient for obtaining stable V_T estimates (Terry et al., 2009).

In addition, the injected doses used in previous studies were generally approximately twice as high as the doses used in our study, up to 750 MBq of [^{11}C]MePPEP (Terry et al., 2009). We achieved reliable receptor availability estimation using only 370 MBq, entailing an effective dose of just ~1.7 mSv per scan (Terry et al., 2010a). We had previously observed that both image quality and the reliability of blood data measurements were lower when injected doses of a radioligand with similarly slow kinetics were lowered to ~180 MBq (Hammers et al., 2007a). In our hands, mSUVs – using only tissue data – yielded excellent test–retest properties and differentiation between regions, with the highest pallidum/pons ratio of all methods. The fact that excellent reliability and differentiation between regions with high and low receptor concentrations (Herkenham et al., 1990) could be achieved with methods using metabolite-corrected arterial plasma input functions suggests the reliability of the blood measurements.

Because arterial cannulations require skilled personnel and involve discomfort and small risks to volunteers and patients, non-invasive PET studies are usually preferred in research studies, and even more so in a clinical environment. Methods using a reference region devoid of the studied receptor are needed for full quantification in the absence of an input function. However, CB_1 receptors are present throughout the brain, and a true reference region does not exist. Here we used the pons as a pseudo-reference region. It has low CB_1 receptor concentration (Herkenham et al., 1990; Irving et al., 2002; Terry et al., 2009; Yasuno et al., 2008), motivating this attempt despite some specific binding (Terry et al., 2009; Yasuno et al., 2008). We were unable to achieve reliable data. The application of more sophisticated pseudo-reference region approaches as described in recent studies (Turkheimer et al., 2012) might improve on these results. However, we note that the pons tissue data (i.e. mSUV) measurements were far less reliable than measurements elsewhere. Even small variations in the amount of specific binding between individuals may thus have a large influence on the radioactivity concentration in this region, with resulting low reliability for the SRTM.

This is the first study to apply model-free analyses (spectral analysis with or without rank shaping regularisation) to quantify cannabinoid receptor availability using [^{11}C]MePPEP PET. These have the advantage of being 'data-driven' rather than requiring an a priori model selection. We additionally describe the first voxel-wise quantification of [^{11}C]MePPEP, yielding parametric V_T images with high corresponding regional ICCs. Spectral analysis does not require a priori assumptions regarding the number of components, compartments, or distribution of receptors. Spectral analysis estimations require compartmental systems that are strongly connected, have exchange of material with the

Table 11

Intraclass correlation coefficients (ICCs) for subjects' volume of distribution (V_T) and/or binding potential (BP) obtained with the different methods. The ratio V_T /BP of a high binding region (pallidum) over that of a low-binding region (pons) is also given. ACG = anterior cingulate gyrus, IFG = inferior frontal gyrus, caudate = caudate nucleus, pallidum = globus pallidus, accumbens = nucleus accumbens. ROI = region-of-interest, SD = standard deviation, NA = not applicable.

Method	2kbv	4kbv	SA-ROIs	SA-maps	RS-SA	SRTM	mSUV
Parameter	V_T	V_T	V_T	V_T	V_T	BP_{ND}	kBq/ml
Sampling	ROI on dynamic images	ROI on dynamic images	ROI on dynamic images	ROI on parametric maps	ROI on dynamic images	ROI on dynamic images	ROI on summed images
Hippocampus	0.88	−0.05	0.87	0.87	0.81	−0.06	0.84
ACG	0.76	0.23	0.74	0.85	0.86	0.50	0.86
IFG	0.83	0.13	0.71	0.85	0.85	−0.29	0.86
Caudate	0.85	−0.13	0.74	0.81	0.82	0.06	0.79
Pallidum	0.70	−0.03	0.85	0.83	0.77	0.27	0.84
Accumbens	0.69	−0.06	0.80	0.83	0.73	−0.15	0.80
Thalamus	0.89	0.49	0.70	0.76	0.85	0.19	0.83
Pons	0.95	0.50	0.67	0.81	0.90	NA	0.47
Mean ± SD	0.82 ± 0.09	0.14 ± 0.25	0.76 ± 0.07	0.83 ± 0.03	0.82 ± 0.05	0.07 ± 0.27	0.79 ± 0.13
Ratio pallidum/pons	3.6	2.0	2.6	3.6	2.4	NA	4.2

environment confined to a single compartment, and do not contain cycles, i.e., there is no possibility for material to pass from one compartment through two or more compartments back to the initial compartment (Schmidt, 1999). SA cannot be used to estimate reference region models because the fit assumes a sum of positive series of convolution integrals of the input function. This last condition is relaxed in Rank-Shaping SA.

We do not expect any biases when spectral analysis is applied to data from participants who are not healthy controls. SA has been used successfully in several patient populations.

The improved ICC measures of SA methodologies over compartmental ones indicate a complex compartmentalisation of the underlying receptor distribution. CB1 receptors can be found on neurons, astrocytes, and also the vascular endothelium. Compartmental models usually assume that a single concentration represents the free-in-tissue tracer compartment. This concentration in reality is the average of concentrations of the free radioligand in different tissue environments, as there will be a gradient across different cellular elements. This will cause an apparent change in affinity of the tracer depending on the target cell (Delforge et al., 1996). Spectral analysis, which does not depend on a free compartmental structure, has more flexibility in dealing with such a complex signal.

A major difference relative to the previous test–retest study (Terry et al., 2009) is the lack of reliability of V_T estimates obtained with the two-tissue compartment model (4kbv) in our study, as well as good reliability for V_T estimates obtained using the one-tissue compartment model 2kbv, whereas this had yielded poor fits for Terry et al. (2009). This might relate to longer scanning time and nearly twice the injected dose in the former study. An additional major difference in the models is that we estimated the blood volume contribution, whereas this had been set to 5% in the previous study. Of note, for a similar time interval our standardized uptake values are comparable to those of Terry et al. (2009).

We did not collect data from the female participants concerning the stage of their menstrual cycle on the day of scanning. Here, when this was tested for the “classic” spectral analysis (parametric maps) method, there was no significant between-subject influence of gender on the V_T s; nor was there a significant interaction between gender and test–retest condition. Whilst further investigation is required, we therefore hypothesise that the menstrual cycle has a minimal effect on the variability of [11 C]MePPEP V_T in human females.

We did not calculate the parent tracer free fraction, which may be important (Terry et al., 2010a; Terry et al., 2010b; Yasuno et al., 2008). However, our result of good reproducibility with tissue-only data (mSUV) and even better reproducibility with modelling approaches using the arterial input data suggests that this omission did not have an adverse effect.

In conclusion, quantification of CB₁ receptor availability showed good-to-excellent reproducibility with selected kinetic and model-free analyses, whether applied on a region-of-interest or voxel-wise basis. [11 C]MePPEP PET is well-placed as a tool to investigate CB₁ receptor-mediated neurotransmission in health and neuropsychiatric disease.

Acknowledgments

We thank the staff of Hammersmith Imanet Limited and the Hammersmith Hospital MRI Unit for their assistance with data acquisition and preparation. This study was supported by the MRC Clinical Sciences Centre. Authors affiliated with ^a are grateful for support from the Department of Health NIHR Biomedical Research Centre's funding scheme. CJM was supported by an MRC Doctoral Training Account (3 + 1) studentship that was awarded by Imperial College London. JSD and MJK were supported by the Epilepsy Society, UCL, UCL Hospitals and UCLH/UCL Biomedical Research Centre. AH was supported by an MRC Clinician Scientist Fellowship (G108/585) and the Neurodis Foundation.

References

- Ahmad, R., Goffin, K., Van den Stock, J., De Winter, F.L., Cleeren, E., Bormans, G., Tournoy, J., Persoons, P., Van Laere, K., Vandenberghe, M., 2014. In vivo type 1 cannabinoid receptor availability in Alzheimer's disease. *Eur. Neuropsychopharmacol.* 24, 242–250.
- Allen, E.V., 1929. Thromboangiitis obliterans: methods of diagnosis of chronic occlusive arterial lesions distal to the wrist with illustrative cases. *Am. J. Med. Sci.* 178, 237–244.
- Aston, J.A.D., Worsley, K.J., Gunn, R.N., 2001. RPM statistics — a statistical tool for receptor parametric mapping. *Neuroimage* 13, 65–65.
- Bossong, M.G., van Berckel, B.N.M., Boellaard, R., Zuurman, L., Schuit, R.C., Windhorst, A.D., van Gerven, J.M.A., Ramsey, N.F., Lammertsma, A.A., Kahn, R.S., 2009. Delta 9-tetrahydrocannabinol induces dopamine release in the human striatum. *Neuropsychopharmacology* 34, 759–766.
- Burns, H.D., Van Laere, K., Sanabria-Bohorquez, S., Hamill, T.G., Bormans, G., Eng, W.S., Gibson, R., Ryan, C., Connolly, B., Patel, S., Krause, S., Vanko, A., Van Hecken, A., Dupont, P., De Lepeleire, I., Rothenberg, P., Stoch, S.A., Cote, J., Hagmann, W.K., Jewell, J.P., Lin, L.S., Liu, P., Goulet, M.T., Gottesdiener, K., Wagner, J.A., de Hoon, J., Mortelmans, L., Fong, T.M., Hargreaves, R.J., 2007. F-18 MK-9470, a positron emission tomography (PET) tracer for in vivo human PET brain imaging of the cannabinoid-1 receptor. *Proc. Natl. Acad. Sci. U. S. A.* 104, 9800–9805.
- Cable, D.G., Mullany, C.J., Schaff, H.V., 1999. The Allen test. *Ann. Thorac. Surg.* 67, 876–877.
- Charalambous, A., Marciniak, G., Shiue, C.Y., Dewey, S.L., Schlyer, D.J., Wolf, A.P., Makriyannis, A., 1991. PET studies in the primate brain and distribution in mice using (–)-5'-¹⁸F-DELTA-8-THC. *Pharmacol. Biochem. Behav.* 40, 503–507.
- Cunningham, V.J., Jones, T., 1993. Spectral-analysis of dynamic pet studies. *J. Cereb. Blood Flow Metab.* 13, 15–23.
- Cunningham, V.J., Hume, S.P., Price, G.R., Ahier, R.G., Cremer, J.E., Jones, A.K.P., 1991. Compartmental analysis of diprenorphine binding to opiate receptors in the rat in vivo and its comparison with equilibrium data in vitro. *J. Cereb. Blood Flow Metab.* 11, 1–9.
- Cunningham, V.J., Ashburner, J., Byrne, H., Jones, T., 1993. Use of spectral-analysis to obtain parametric images from dynamic pet studies. *Quantification of Brain Function*, 1030, pp. 101–111.
- Defrise, M., Kinahan, P.E., Townsend, D.W., Michel, C., Sibomana, M., Newport, D.F., 1997. Exact and approximate rebinning algorithms for 3-D PET data. *IEEE Trans. Med. Imaging* 16, 145–158.
- Delforge, J., Syrota, A., Bendriem, B., 1996. Concept of reaction volume in the in vivo ligand-receptor model. *J. Nucl. Med.* 37, 118–125.
- Devane, W.A., Dysarz, F.A., Johnson, M.R., Melvin, L.S., Howlett, A.C., 1988. Determination and characterization of a cannabinoid receptor in rat-brain. *Mol. Pharmacol.* 34, 605–613.
- Devane, W.A., Hanus, L., Breuer, A., Pertwee, R.G., Stevenson, L.A., Griffin, G., Gibson, D., Mandelbaum, A., Etinger, A., Mechoulam, R., 1992. Isolation and structure of a brain constituent that binds to the cannabinoid receptor. *Science* 258, 1946–1949.
- Finnema, S.J., Donohue, S.R., Zoghbi, S.S., Brown, A.K., Gulyas, B., Innis, R.B., Halldin, C., Pike, V.W., 2009. Evaluation of (11)C PipiSB and (18)F PipiSB in monkey as candidate radioligands for imaging brain cannabinoid type-1 receptors in vivo. *Synapse* 63, 22–30.
- Gatley, S.J., Gifford, A.N., Volkow, N.D., Lan, R.X., Makriyannis, A., 1996. I-123-labeled AM251: a radioiodinated ligand which binds in vivo to mouse brain cannabinoid CB1 receptors. *Eur. J. Pharmacol.* 307, 331–338.
- Gatley, S.J., Lan, R., Volkow, N.D., Pappas, N., King, P., Wong, C.T., Gifford, A.N., Pyatt, B., Dewey, S.L., Makriyannis, A., 1998. Imaging the brain marijuana receptor: development of a radioligand that binds to cannabinoid CB1 receptors in vivo. *J. Neurochem.* 70, 417–423.
- Goffin, K., Van Paesschen, W., Van Laere, K., 2011. In vivo activation of endocannabinoid system in temporal lobe epilepsy with hippocampal sclerosis. *Brain* 134, 1033–1040.
- Gousias, I.S., Rueckert, D., Heckemann, R.A., Dyet, L.E., Boardman, J.P., Edwards, A.D., Hammers, A., 2008. Automatic segmentation of brain MRIs of 2-year-olds into 83 regions of interest. *NeuroImage* 40, 672–684.
- Griffin, G., Atkinson, P.J., Showalter, V.M., Martin, B.R., Abood, M.E., 1998. Evaluation of cannabinoid receptor agonists and antagonists using the guanosine-5'- γ -O-(3-S-3-thio)-triphosphate binding assay in rat cerebellar membranes. *J. Pharmacol. Exp. Ther.* 285, 553–560.
- Gunn, R.N., Lammertsma, A.A., Hume, S.P., Cunningham, V.J., 1997. Parametric imaging of ligand-receptor binding in PET using a simplified reference region model. *NeuroImage* 6, 279–287.
- Gunn, R.N., Sargent, P.A., Bench, C.J., Rabiner, E.A., Osman, S., Pike, V.W., Hume, S.P., Grasby, P.M., Lammertsma, A.A., 1998. Tracer kinetic modeling of the 5-HT1A receptor ligand [carbonyl-¹¹C]WAY-100635 for PET. *NeuroImage* 8, 426–440.
- Gunn, R.N., Gunn, S.R., Cunningham, V.J., 2001. Positron emission tomography compartmental models. *J. Cereb. Blood Flow Metab.* 21, 635–652.
- Hamill, T.G., Lin, L.S., Hagmann, W., Liu, P., Jewell, J., Sanabria, S., Eng, W., Ryan, C., Fong, T.M., Connolly, B., Vanko, A., Hargreaves, R., Goulet, M.T., Burns, H.D., 2009. PET imaging studies in rhesus monkey with the cannabinoid-1 (CB1) receptor ligand (11)C CB-119. *Mol. Imaging Biol.* 11, 246–252.
- Hammers, A., Allom, R., Koeppe, M.J., Free, S.L., Myers, R., Lemieux, L., Mitchell, T.N., Brooks, D.J., Duncan, J.S., 2003. Three-dimensional maximum probability atlas of the human brain, with particular reference to the temporal lobe. *Hum. Brain Mapp.* 19, 224–247.
- Hammers, A., Asselin, M.-C., Turkheimer, F.E., Hinz, R., Osman, S., Hotton, G., Brooks, D.J., Duncan, J.S., Koeppe, M.J., 2007a. Balancing bias, reliability, noise properties and the need for parametric maps in quantitative ligand PET: [11 C]diprenorphine test-retest data. *NeuroImage* 38, 82–94.

- Hammers, A., Asselin, M.C., Hinz, R., Kitchen, I., Brooks, D.J., Duncan, J.S., Koeppe, M.J., 2007b. Upregulation of opioid receptor binding following spontaneous epileptic seizures. *Brain* 130, 1009–1016.
- Hammers, A., Panagoda, P., Heckemann, R.A., Kelsch, W., Turkheimer, F.E., Brooks, D.J., Duncan, J.S., Koeppe, M.J., 2008. [C-11] Flumazenil PET in temporal lobe epilepsy: do we need an arterial input function or kinetic modeling? *J. Cereb. Blood Flow Metab.* 28, 207–216.
- Hampson, R.E., Sweatt, A.J., Goonawardena, A.V., Song, D., Chan, R.H.M., Marmarelis, V.Z., Berger, T.W., Deadwyler, S.A., 2011. Memory encoding in hippocampal ensembles is negatively influenced by cannabinoid CB1 receptors. *Behav. Pharmacol.* 22, 335–346.
- Heckemann, R.A., Hajnal, J.V., Aljabar, P., Rueckert, D., Hammers, A., 2006. Automatic anatomical brain MRI segmentation combining label propagation and decision fusion. *NeuroImage* 33, 115–126.
- Heckemann, R.A., Keihaninejad, S., Aljabar, P., Rueckert, D., Hajnal, J.V., Hammers, A., Alzheimer's Disease Neuroimaging Initiative, 2010. Improving intersubject image registration using tissue-class information benefits robustness and accuracy of multi-atlas based anatomical segmentation. *NeuroImage* 51, 221–227.
- Heckemann, R.A., Keihaninejad, S., Aljabar, P., Gray, K.R., Nielsen, C., Rueckert, D., Hajnal, J.V., Hammers, A., 2011. Automatic morphometry in Alzheimer's disease and mild cognitive impairment. *NeuroImage* 56, 2024–2037.
- Herkenham, M., Lynn, A.B., Little, M.D., Johnson, M.R., Melvin, L.S., DeCosta, B.R., Rice, K.C., 1990. Cannabinoid receptor localization in brain. *Proc. Natl. Acad. Sci. U. S. A.* 87, 1932–1936.
- Horti, A.G., Fan, H., Kuwabara, H., Hilton, J., Ravert, H.T., Holt, D.P., Alexander, M., Kumar, A., Rahmim, A., Scheffel, U., Wong, D.F., Dannals, R.F., 2006. C-11-JHU75528: A radiotracer for PET imaging of CB1 cannabinoid receptors. *J. Nucl. Med.* 47, 1689–1696.
- Huang, S.C., Phelps, M.E., Hoffman, E.J., Sideris, K., Selin, C.J., Kuhl, D.E., 1980. Non-invasive determination of local cerebral metabolic-rate of glucose in man. *Am. J. Physiol.* 238, E69–E82.
- Innis, R.B., Cunningham, V.J., Delforge, J., Fujita, M., Giedde, A., Gunn, R.N., Holden, J., Houle, S., Huang, S.C., Ichise, M., Lida, H., Ito, H., Kimura, Y., Koeppe, R.A., Knudsen, G.M., Knuuti, J., Lammertsma, A.A., Laruelle, M., Logan, J., Maguire, R.P., Mintun, M.A., Morris, E.D., Parsey, R., Price, J.C., Slifstein, M., Sossi, V., Suhara, T., Votaw, J.R., Wong, D.F., Carson, R.E., 2007. Consensus nomenclature for in vivo imaging of reversibly binding radioligands. *J. Cereb. Blood Flow Metab.* 27, 1533–1539.
- Irving, A.J., Rae, M.G., Coutts, A.A., 2002. Cannabinoids on the brain. *Sci. World J.* 2, 632–648.
- Jones, A.K.P., Cunningham, V.J., Hakawa, S.K., Fujiwara, T., Qi, L.Y., Luthra, S.K., Ashburner, J., Osman, S., Jones, T., 1994. Quantification of [C-11] diprenorphine cerebral kinetics in man acquired by PET using presaturation, pulse-chase and tracer-only protocols. *J. Neurosci. Methods* 51, 123–134.
- Katona, I., Freund, T.F., 2008. Endocannabinoid signaling as a synaptic circuit breaker in neurological disease. *Nat. Med.* 14, 923–930.
- MacLennan, R.N., 1993. Interrater reliability with SPSS for Windows 5.0. *Am. Stat.* 47, 292–296.
- Matsuda, L.A., Lolait, S.J., Brownstein, M.J., Young, A.C., Bonner, T.I., 1990. Structure of a cannabinoid receptor and functional expression of the cloned cDNA. *Nature* 346, 561–564.
- Petitot, F., Marin, L., Doble, A., 1996. Biochemical and pharmacological characterization of cannabinoid binding sites using H-3 SR141716A. *Neuroreport* 7, 789–792.
- Portney, L.G., Watkins, M.P., 2009. *Foundations of Clinical Research: Applications to Practice*. Prentice Hall, Upper Saddle River, NJ pp. 560–567.
- Schmidt, K., 1999. Which linear compartmental systems can be analyzed by spectral analysis of PET output data summed over all compartments? *J. Cereb. Blood Flow Metab.* 19, 560–569.
- Slogoff, S., Keats, A.S., Arlund, C., 1983. On the safety of radial artery cannulation. *Anesthesiology* 59, 42–47.
- Studholme, C., Hill, D.L., Hawkes, D.J., 1996. Automated 3-D registration of MR and CT images of the head. *Med. Image Anal.* 1, 163–175.
- Terry, G.E., Liow, J.S., Chernet, E., Zoghbi, S.S., Phebus, L., Felder, C.C., Tauscher, J., Schaus, J.M., Pike, V.W., Halldin, C., Innis, R.B., 2008. Positron emission tomography imaging using an inverse agonist radioligand to assess cannabinoid CB1 receptors in rodents. *NeuroImage* 41, 690–698.
- Terry, G.E., Liow, J.S., Zoghbi, S.S., Hirvonen, J., Farris, A.G., Lerner, A., Tauscher, J.T., Schaus, J.M., Phebus, L., Felder, C.C., Morse, C.L., Hong, J.S., Pike, V.W., Halldin, C., Innis, R.B., 2009. Quantitation of cannabinoid CB(1) receptors in healthy human brain using positron emission tomography and an inverse agonist radioligand. *NeuroImage* 48, 362–370.
- Terry, G., Hirvonen, J., Liow, J.-S., Seneca, N., Tauscher, J., Schaus, J., Phebus, L., Felder, C., Morse, C., Pike, V., Halldin, C., Innis, R., 2010a. Biodistribution and dosimetry in humans of two inverse agonists to image cannabinoid CB1 receptors using positron emission tomography. *Eur. J. Nucl. Med. Mol. Imaging* 37, 1499–1506.
- Terry, G.E., Hirvonen, J., Liow, J.S., Zoghbi, S.S., Gladding, R., Tauscher, J.T., Schaus, J.M., Phebus, L., Felder, C.C., Morse, C.L., Donohue, S.R., Pike, V.W., Halldin, C., Innis, R.B., 2010b. Imaging and quantitation of cannabinoid CB(1) receptors in human and monkey brains using (18)F-labeled inverse agonist radioligands. *J. Nucl. Med.* 51, 112–120.
- Turkheimer, F., Moresco, R.M., Lucignani, G., Sokoloff, L., Fazio, F., Schmidt, K., 1994. The use of spectral analysis to determine regional cerebral glucose utilization with positron emission tomography and [¹⁸F]fluorodeoxyglucose: theory, implementation, and optimization procedures. *J. Cereb. Blood Flow Metab.* 14 (3), 406–422.
- Turkheimer, F.E., Brett, M., Visvikis, D., Cunningham, V.J., 1999. Multiresolution analysis of emission tomography images in the wavelet domain. *J. Cereb. Blood Flow Metab.* 19, 1189–1208.
- Turkheimer, F.E., Hinz, R., Gunn, R.N., Aston, J.A.D., Gunn, S.R., Cunningham, V.J., 2003. Rank-shaping regularization of exponential spectral analysis for application to functional parametric mapping. *Phys. Med. Biol.* 48, 3819–3841.
- Turkheimer, F.E., Selvaraj, S., Hinz, R., Murthy, V., Bhagwagar, Z., Grasby, P., Howes, O., Rosso, L., Bose, S.K., 2012. Quantification of ligand PET studies using a reference region with a displaceable fraction: application to occupancy studies with [(11)C]-DASB as an example. *J. Cereb. Blood Flow Metab.* 32, 70–80.
- Van Laere, K., Casteels, C., Dhollander, I., Goffin, K., Grachev, I., Bormans, G., Vandenberghe, W., 2010. Widespread decrease of type 1 cannabinoid receptor availability in Huntington disease in vivo. *J. Nucl. Med.* 51, 1413–1417.
- Watabe, H., Ikoma, Y., Kimura, Y., Naganawa, M., Shidahara, M., 2006. PET kinetic analysis – compartmental model. *Ann. Nucl. Med.* 20, 583–588.
- Wong, D.F., Kuwabara, H., Horti, A.G., Raymond, V., Brasic, J., Guevara, M., Ye, W., Dannals, R.F., Ravert, H.T., Nandi, A., Rahmim, A., Ming, J.E., Grachev, I., Roy, C., Cascella, N., 2010. Quantification of cerebral cannabinoid receptors subtype 1 (CB1) in healthy subjects and schizophrenia by the novel PET radioligand [11C]OMAR. *NeuroImage* 52, 1505–1513.
- Yasuno, F., Brown, A.K., Zoghbi, S.S., Krushinski, J.H., Chernet, E., Tauscher, J., Schaus, J.M., Phebus, L.A., Chesterfield, A.K., Felder, C.C., Gladding, R.L., Hong, J., Halldin, C., Pike, V.W., Innis, R.B., 2008. The PET radioligand [C-11]MePPEP binds reversibly and with high specific signal to cannabinoid CB1 receptors in nonhuman primate brain. *Neuropsychopharmacology* 33, 259–269.